Ultrahigh cooperativity interactions between magnons and resonant photons in a YIG sphere

J. Bourhill,* N. Kostylev, M. Goryachev, D. L. Creedon, and M. E. Tobar
ARC Centre of Excellence for Engineered Quantum Systems, University of Western Australia, 35 Stirling Highway, Crawley WA 6009, Australia

(Received 3 January 2016; published 25 April 2016)

Resonant photon modes of a 5-mm-diameter yttrium iron garnet (YIG) sphere loaded in a cylindrical cavity in the 10–30-GHz frequency range are characterized as a function of applied dc magnetic field at millikelvin temperatures. The photon modes are confined mainly to the sphere and exhibited large mode filling factors in comparison to previous experiments, allowing ultrastrong coupling with the magnon spin-wave resonances. The largest observed coupling between photons and magnons is $2g/2\pi = 7.11$ GHz for a 15.5-GHz mode, corresponding to a cooperativity of $C = 1.51 \pm 0.47 \times 10^7$. Complex modifications, beyond a simple multioscillator model, of the photon mode frequencies were observed between 0 and 0.1 T. Between 0.4 and 1 T, degenerate resonant photon modes were observed to interact with magnon spin-wave resonances with different coupling strengths, indicating time-reversal symmetry breaking due to the gyrotropic permeability of YIG. Bare dielectric resonator mode frequencies were determined by detuning magnon modes to significantly higher frequencies with strong magnetic fields. By comparing measured mode frequencies at 7 T with finite element modeling, a bare dielectric permittivity of 15.96 ± 0.02 of the YIG crystal has been determined at about 20 mK.

DOI: 10.1103/PhysRevB.93.144420

I. INTRODUCTION

Hybrid photon-magnon systems in ferromagnetic spheres have recently emerged as a promising approach towards coherent information processing [1–8]. Due to the large exchange interaction between spins in ferromagnets, they will lock together to form a macrospin that can be utilized for coherent information processing protocols [8,9]. The quantized excitation of the collective spin is referred to as a magnon. Yttrium iron garnet (YIG)–based magnon systems are attractive due to very high spin density, resulting in significant cooperativity as well as relatively narrow linewidths [4,5,10,11]. Furthermore, due to the possibility of coupling magnon modes to photons at optical frequencies [10–13], magnon systems may be considered as a candidate for coherent conversion of microwave and optical photons [10,11]. In addition, magnons interact with elastic waves [14,15], opening a window for combining mechanical and magnetic systems. These systems therefore possess great potential as an information transducer that mediates interconversion between information carriers of different physical natures, thus establishing a novel approach to hybrid quantum systems [9,16–18].

Among all magnon systems the central role is devoted to YIG, a material that possesses exceptional magnetic and microwave properties and has been used in microwave systems such as tuneable oscillators and filters for many decades [19,20]. However, only recently Soykal and Flatté proposed and modelled the photon-magnon interaction based on YIG nanospheres with application to quantum systems [21,22]. As predicted by the authors, extremely large coupling rates g could be achieved in YIG spheres, which is favorable for coherent information exchange and was demonstrated experimentally later [4,5,23]. For these experiments, the interaction is observed between photon and magnon resonances created respectively by photon cavity boundary conditions and spin precession under external dc magnetic field. A commonly used method is to place a relatively small YIG sphere in a local maxima of the magnetic field inside a much larger microwave cavity. This is done to achieve quasiuniform distribution of the cavity field over the sphere volume to avoid spurious magnon modes. Cavities can take oval [3,4] or spherical shapes [21,22,24], and even reentrant cavities with multiple posts have been used in an attempt to focus the microwave energy over the sphere [5,23]. In this work we investigate a completely different regime in which the magnon and photon wavelengths are comparable, leading to considerably larger coupling strengths but additional couplings to higher-order modes. In general, for this case the strength of the photon-magnon interaction will be determined by an overlap integral of the two respective mode shape functions. Given that the magnon mode shape is limited to the sphere's volume, this integral will be maximized when the photon mode is confined to the same volume. To achieve the latter, we utilize an exceptionally large YIG sphere with diameter $d = 5$ mm, matching magnon and microwave photon mode volumes, unlike previous microwave cavity experiments.

In order to investigate this regime we use common microwave spectroscopy techniques [5,23,25–28] to directly observe the mode splitting caused by the magnon interaction to determine the coupling values. Similar systems have been extensively utilized not only in the field of spintronics to investigate the interaction between microwave photons and paramagnetic spin ensembles [25–29], but also to realize optical comb generation [30], ultra-low-threshold lasing [31], cavity-assisted cooling, control and measurement of optomechanical systems [32,33], and extremely stable cryogenic sapphire oscillator clock technology [34,35]. To date, exciting internal, highly confined photonic modes in a YIG sphere have only recently been demonstrated in the optical regime using whispering gallery modes (WGMs) [10,11] but have never before been achieved in the microwave domain. This is due to

*jeremy.bourhill@uwa.edu.au

the typical sub-millimeter diameter of the spheres. As such, interactions with magnons must be observed via Brillouin scattering [36], which has yielded high quality factors and also demonstrated a pronounced nonreciprocity and asymmetry in the sideband signals generated by the magnon-induced scattering.

Extremely large mode splittings ($g/\omega > 0.1$) cause simultaneous coupling to a higher density of modes, with an overlap of avoided level crossings. Therefore, the model proposed by Soykal and Flatté [21] becomes no longer applicable, as it assumes the interaction occurs between a single photonic and magnon mode. More recently, a paper by Rameshti *et al.* [24] simulated a similar scenario of the presented experiment in which the ferromagnetic sphere is itself the microwave cavity. Our observed results may appear to be in good agreement with this work's predictions; however, what is apparent is that in this specialized case, one must consider more than just the magnetostatic, uniform Kittel magnon mode, a limitation of [24]. Indeed, due to the nonuniformity of both the microwave mode magnetic field energy density across the sphere, which is unique to this experiment, and the nonuniformity of the sphere parameters arising due to cryogenic cooling, the assumption that only the uniform Kittel magnon resonance participates is no longer valid. Despite this, in this paper we use a two-mode model to obtain estimations of coupling strengths and demonstrate how this results in inconsistent susceptibility values.

II. PHYSICAL REALIZATION

The $d = 5$ mm YIG sphere was manufactured by Ferrisphere, Inc., with a quoted room temperature saturation magnetization of $\mu_0 M = 0.178$ T. It is placed on a small sapphire disk, with a concavity etched out using a diamond-tipped ball grinder, to keep the sphere from rolling out of position and reduce dielectric losses that would arise if the YIG were in direct contact with the conductive copper housing. Sapphire was chosen over Teflon as an intermediary between the YIG and copper to improve the thermal conductivity to the sphere.

Together, the sapphire and YIG are housed inside a copper cavity with dimensions specified in Fig. 1. A loop probe constructed from flexible subminiature version A cable launchers is used to input microwaves and a second is used to make measurements, allowing the determination of S parameters. The entire cavity is cooled to about 20 mK by means of a dilution refrigerator (DR) with a cooling power of about 500 μW at 100 mK. The cavity is attached to a copper rod bolted to the mixing chamber stage of the DR that places it at the field center of a 7-T superconducting magnet whose applied field is oriented in the z direction of the cavity. The magnet is attached to the 4-K stage of the DR, with the copper cavity mounted within a radiation shield of approximately 100 mK that sits within the bore of the magnet.

III. EXPERIMENTAL OBSERVATIONS

The transmission spectrum of the YIG was recorded for dc magnetic fields swept from 0 to 7 T using a vector network analyzer (VNA), with partial results shown in Fig. 2. A host

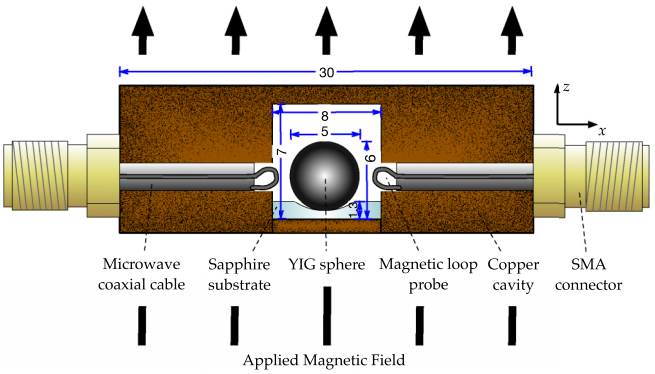

FIG. 1. Cross section of the copper cavity that houses the 5-mm YIG sphere. The sphere sits on a sapphire disk, and microwaves are coupled in and out of it via loop probes which produce and detect an H_ϕ component. A variable dc magnetic field is applied along the z axis.

of magnon resonances/higher-order magnon polaritons can be observed originating from (0 T, 0 GHz) with an approximate gradient of 28 GHz/T. The more-or-less horizontal lines approaching the magnon resonances from either side correspond to resonant photon modes of the sphere. Importantly, we can observe that in the dispersive regime, far removed from any microwave resonant mode, there still exist multiple magnon modes. We observe that the anticrossing gaps are populated by unperturbed modes, which are remnant "tails" of both "higher" and "lower" mode interactions, as predicted by Rameshti *et al.* in the ultrastrong coupling regime [24].

For the remainder of this paper, we will focus on the six lowest frequency photon modes, whose resonant frequencies may only be accurately determined at large magnetic fields, when the entire spin ensemble has been detuned, as shown by Fig. 3.

The modes have been categorized into three distinct classes: mode x is the lowest frequency and lowest Q-factor mode, the two highest Q-factor modes i and ii, and the three remaining highest frequency modes 1, 2, and 3. Their asymptotic frequencies as $B \to 7$ T are summarized in Table I.

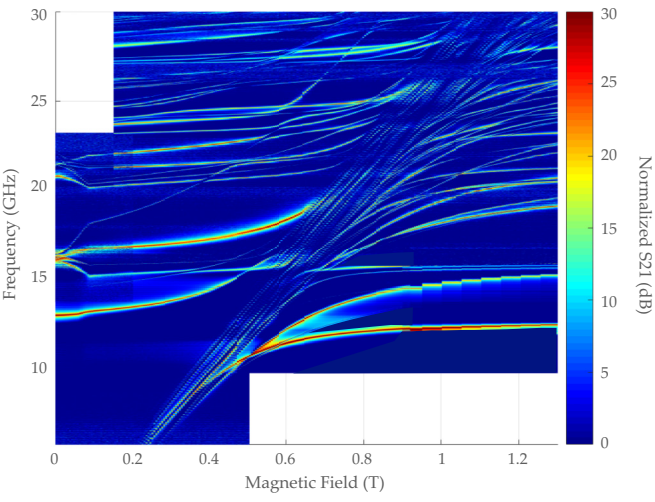

FIG. 2. Transmission data as magnetic field is swept.

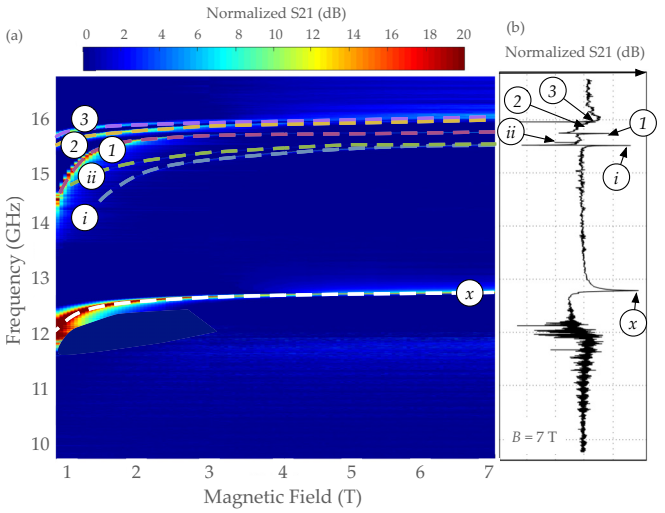

FIG. 3. (a) Asymptotic frequency values of the six lowest-order photon modes as $B \to 7$ T. (b) Transmission spectra at $B = 7$ T, from which mode linewidths may be measured.

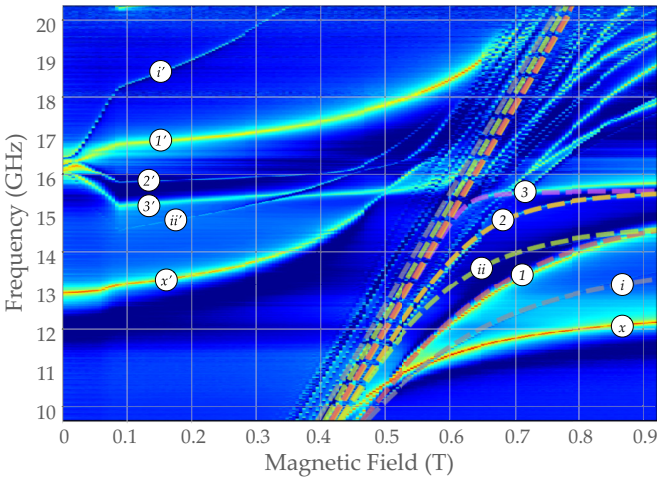

FIG. 4. Two harmonic oscillator models fitting to modes i,ii, 1, 2, and 3. From the curved line shapes, one can determine the coupling value g.

The behavior of these modes as the magnon resonances are tuned via the applied magnetic field is shown in Fig. 4. It has been shown previously [5] that a standard model of two interacting harmonic oscillators can accurately determine the coupling values from such avoided crossings. However, we observe strong distortion at around 0 T, and also an asymmetry of the mode splittings about the central magnon resonances due to the ultrastrong coupling of the photon modes to the magnon modes, as was observed previously in ruby [29]. Therefore we fit only the curves to the right of the magnon resonance. These fits are shown as the dashed lines in Fig. 4. From these fits we can approximate the values of g for each mode, as summarized in Table I. The linewidths Γ_j and frequencies $\omega_j/2\pi$ of the photon modes are determined from the transmission spectra taken at high field values [Fig. 3(b)], while the magnon linewidth $\Gamma_{\rm mag}$ can be determined by analyzing the transmission spectra in the dispersive regime. We take a frequency sweep at $B = 0.247\,5$ T from 5.75 to 9 GHz in order to view the magnon resonance peaks far away from any interaction with the dielectric microwave modes, as shown in Fig. 5. There is a level of variation among the magnon linewidths as calculated by fitting the peaks with Fano resonance fits, as shown in Fig. 6. This variation and the presence of multiple peaks demonstrates the presence of higher-order magnon modes. Taking the average and standard deviation of these linewidths gives a final estimate of magnon linewidth as $\Gamma_{\rm mag}/\pi = 3.247 \pm 0.493$ MHz. Cooperativity is calculated as $C_j = g_j^2/\,\Gamma_{\rm mag}\Gamma_j$.

The cooperativity values in Table I demonstrate that all modes are strongly coupled to the magnons, and all with the exception of modes 2 and 3 are in the ultrastrong coupling regime (i.e., $g_j/\omega_j \geqslant 0.1$ [24]). The largest cooperativity value obtained is that of mode i, which is, to the authors' knowledge, the largest value ever reported to date in any previously studied spin system.

A transmission spectrum taken at $B = 0.642\,5$ T is shown in Fig. 7, demonstrating the mode splitting of mode 1, symmetric about the magnon resonance. Overlaid in red is the bare photon resonance at 7 T, i.e., the microwave mode unperturbed by the magnon modes. From this red curve, $2\Gamma_1/2\pi$ is determined to be 5.355 MHz, as shown in Table I. When one takes the average of $2\Gamma_{\rm mag}/2\pi = 3.247$ MHz and $2\Gamma_1/2\pi$, one obtains the linewidth of the resulting hybrid state when the magnon resonance is tuned coincident in frequency with the photon mode, as depicted by the dashed blue curve in Fig. 7, i.e.,

TABLE I. Measured and calculated results for each mode showing couplings g_j and cooperativities, C_j.

Mode	$\omega_{j\|B\to 7\,\mathrm{T}}/2\pi$ (GHz)	Γ_j/π (MHz)	g_j/π (GHz)	C_j ($\times 10^5$)	g_j/ω_j (%)
x	12.779	11.84	4.79	5.97 ± 1.85	18.7
i	15.506	1.029	7.11	151 ± 47.0	22.9
ii	15.563	1.197	4.19	45.2 ± 14.0	13.5
1	15.732	5.355	6.15	21.8 ± 6.76	19.5
2	15.893	2.965	3.04	9.60 ± 2.98	9.56
3	15.950	2.965	0.78	0.632 ± 0.196	2.45

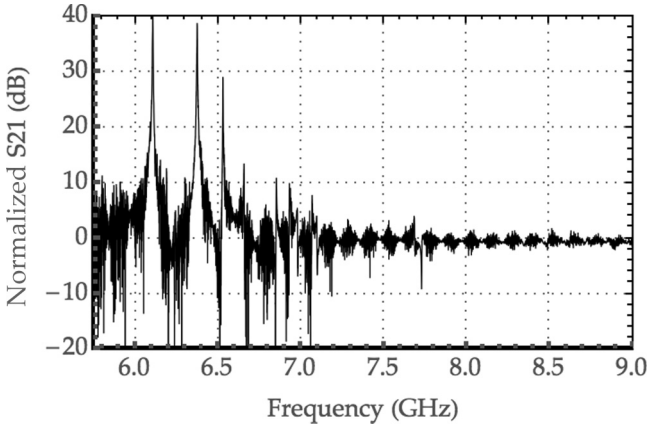

FIG. 5. S21 transmission spectra showing a host of magnon resonance peaks at $B = 0.247\,5$ T.

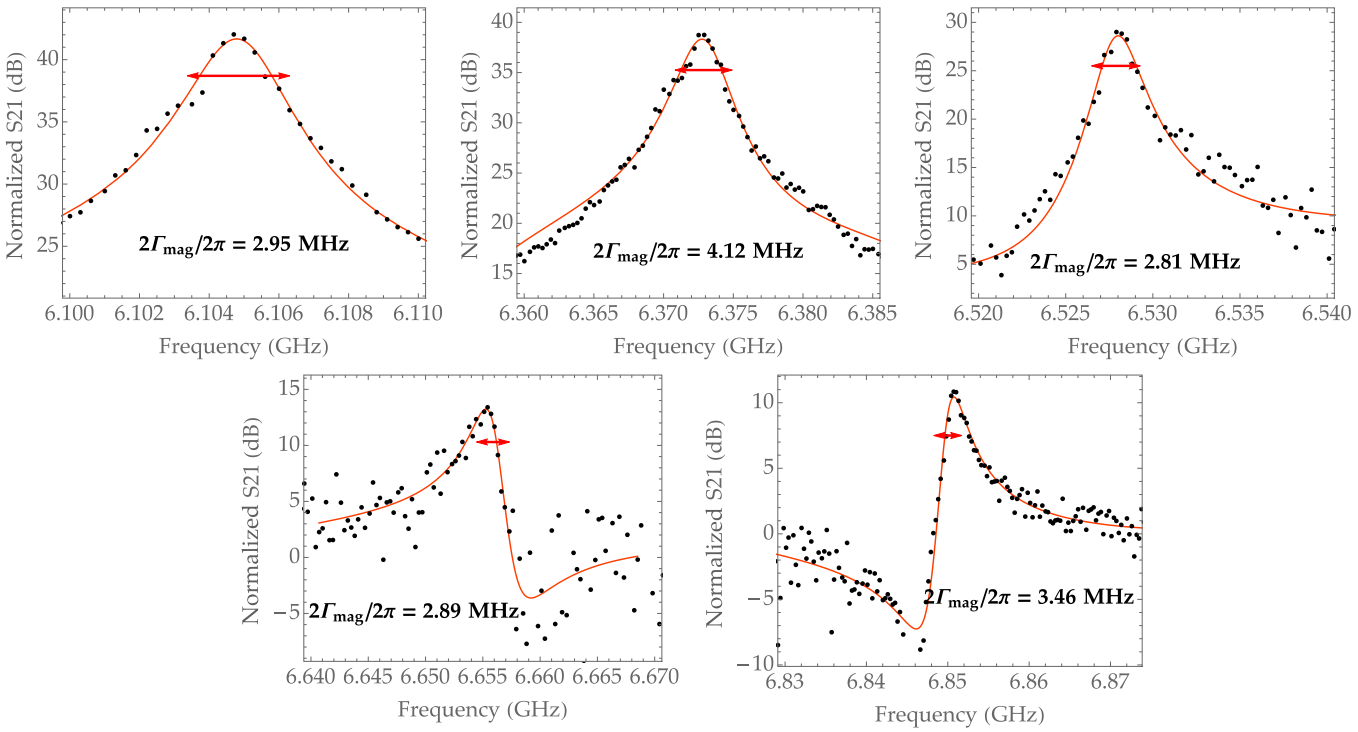

FIG. 6. Fitting the magnon resonances with Fano fits.

~4.4 MHz. This excellent agreement indicates that at this particular B field, mode 1 exists as a hybrid magnon polariton.

At around $B = 0$ T, we observe a severe distortion of the cavity-mode frequency dependence on magnetic field, as demonstrated in Fig. 8. At around 16 GHz, we see there exist five modes, corresponding to modes i,ii, and 1–3, on the "left" side of the magnon resonances. These modes have been given a primed nomenclature to indicate their existence at B fields lower than that required to tune the magnons to their frequencies. This phenomenon has been previously observed in single-crystal yttrium aluminum garnet (YAG) [37] highly doped with rare-earth erbium ions, and is explained by the influence on the ferromagnetic phase of the impurity ions on degenerate modes. The effect can be explained by the influence of the ensemble of strongly coupled spins on the center-propagating waves of the near degenerate mode doublet. For large spin-photon interactions, tails of avoided level crossings (ALCs) from the positive half plane ($B > 0$) should still exist on the negative half plane ($B < 0$) and vice versa, although instead of a gradual change of direction, the system demonstrates an abrupt transition to a "no-coupling" state. It is worth mentioning that such an effect has not been observed in photonic systems interacting with paramagnetic spin ensembles [25,26,38]. In the present case, the effect is

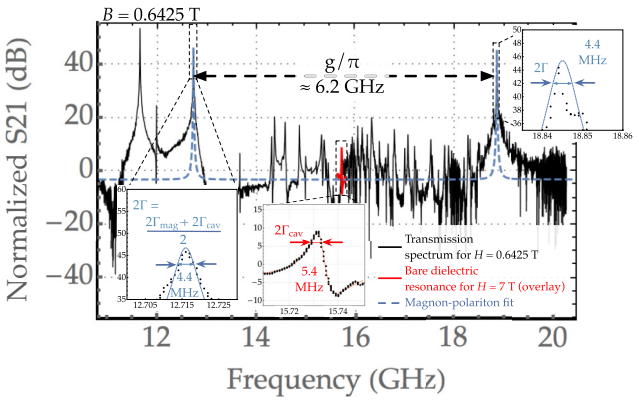

FIG. 7. Transmission spectrum at $B = 0.642\,5$ T. At this applied magnetic field the magnon resonance is tuned coincident in frequency with mode 1, and the strong coupling between the two results in a mode splitting of 6.2 GHz. The high density of resonant peaks in the center of the figure suggests a large number of higher-order magnon modes are present in this system.

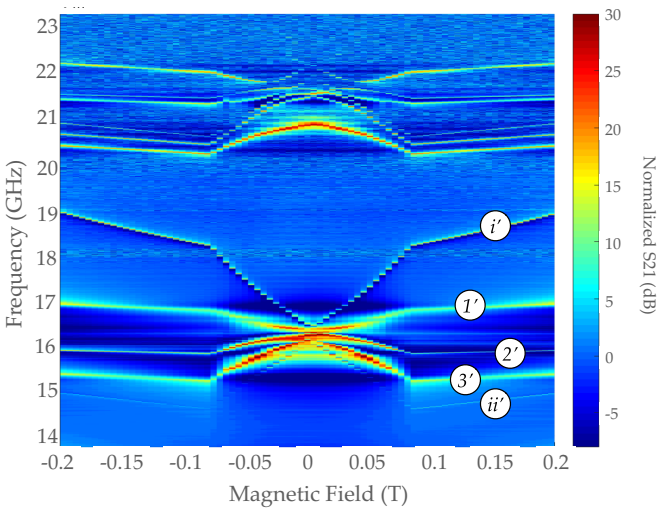

FIG. 8. Behavior of the photon modes around $B = 0$ T, a result of the internal magnetization of YIG.

TABLE II. Comparison of FEM and measured frequencies and hence mode identification.

Mode	f_{meas} (GHz)	f_{sim} (GHz)	(n,m)
x	12.779	12.785	(0,0)
$i\&ii$	15.534	15.286	(1,1)
1	15.732	15.736	(1,0)
2 & 3	15.922	15.921	(1,1)

much more pronounced, with fractional frequency deviations and the magnetic field range of the effect both orders of magnitude larger than observed previously [37], a result of the magnetic spin density.

IV. DISCUSSION

COMSOL 3.5's electromagnetic package was used to model the system. A three dimensional (3D) model was used so as to analyze the degeneracies in the ϕ axis of the dielectric modes. The internal copper wall of the cavity is modeled as a perfect electrical conductor, which, for the purposes of the desired eigenfrequency study, is an appropriate simplification.

The results of the field emission microscopy (FEM) using a value of $\epsilon_{YIG}/\epsilon_0 = 15.965$ and $r' = 3.71$ mm, where r' is the radius of curvature of the sapphire support's concavity, are summarized in Fig. 9 and in Table II. The measured frequency of the doublet modes has been taken as the average of the two constituent's frequencies at $B = 7$ T.

From the FEM and the analytical mode shapes of spherical dielectric resonances described by [39], we can identify mode x as an $n = 0$ mode with no degeneracy. Therefore it is present as a singular resonance. The other five modes appear as $n = 1$ modes. There should exist only a $2n + 1$-fold degeneracy for resonant spherical photon modes, which can be broken by internal impurities or by asymmetric boundary conditions set by a cylindrical enclosure, microwave loop probes, and the sapphire substrate, collectively termed "backscatterers." This degeneracy arises from a Legendre polynomial in the mode's H and E field analytical expressions of the form $P_n^m(\cos\theta)\{^{\cos(m\phi)}_{\sin(m\phi)}\}$, where $m = 0, \ldots, n$. The integers m and n represent the number of maxima of the mode's energy density in the ϕ direction over 180° and the number in the θ direction over 180°, respectively. This would imply that for $n = 1$ we should observe three distinct modes corresponding to a single $(n,m) = (1,0)$ and two $(1,1)$ modes, rather than five modes. However, the FEM demonstrates that the use of the sapphire support base introduces a further degeneracy to the $(1,1)$ modes depending on the amount of field that permeates the sapphire. The modeling predicts four $(1,1)$ modes, existing as two sets of two, which are separated by approximately 500 MHz. This is in fair agreement with the separation of modes i,ii with modes 1–3. Therefore it is apparent that modes i and ii are a doublet pair with $(n,m) = (1,1)$.

Given that modes 2 and 3 approach relatively similar frequencies at high magnetic fields, it is reasonable to assume that these modes correspond to the second $(1,1)$ doublet pair, which FEM predicts will have a larger proportion of microwave field inside the sapphire support. This means that mode 1 must be the $(1,0)$ single mode.

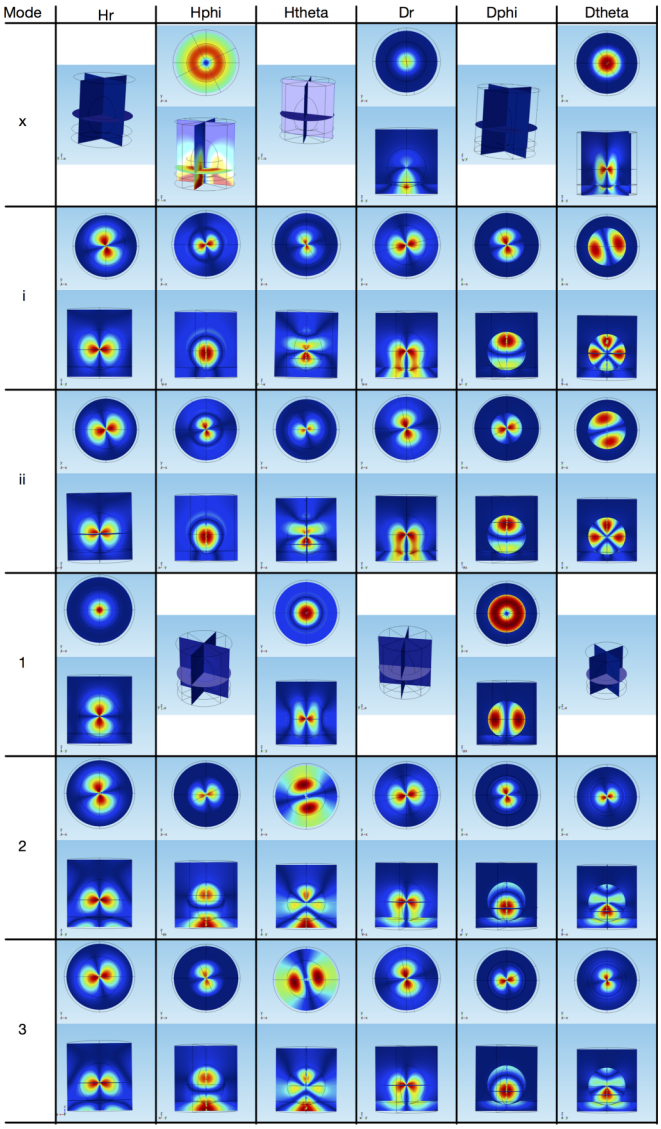

FIG. 9. Spherical coordinate field components of the six lowest dielectric modes in the YIG/sapphire/air system. Each mode is viewed parallel to the z axis (top row) and in the x,y plane (bottom row), except where no field is present. We can readily identify modes x and 1 as (0,0) and (1,0) spherical dielectric modes, respectively. These two modes appear as "pure" dielectric modes containing only three field components. The two doublet modes (i,ii, 2, and 3) appear to contain energy density in all six field components and are greatly affected by the sapphire support, which is what appears to lead to the additional degeneracy, that is, splitting two modes into four modes. From the radial components we can identify these modes as being modified (1,1) spherical dielectric modes.

From Fig. 4, we can see that both the doublet pairs demonstrate a gyrotropic response when interacting with the magnon resonances, i.e., one mode interacts more than its doublet pair. This is a common occurrence in spin ensemble systems and has been observed in paramagnetic systems such as Fe^{3+} in sapphire [26,27,40]. This asymmetric interaction strength for doublet pairs has also been observed in ferromagnets by Krupka *et al.* [41,42] and predicted by Rameshti *et al.* [24], with the latter stating that $g_{n,m=n} > g_{n,m=-n}$, where a different notation to that used here is employed, in

which $m = -n, \ldots, 0, \ldots, n$. The notations are equivalent as an $m = \pm n$ doublet in [24] corresponds to a $\{^{\cos(m\phi)}_{\sin(m\phi)}\}$ doublet pair here.

The gyrotropic response is a result of the anisotropy of a ferromagnet's permeability tensor, the same reason why these materials are used in circulators. The permeability tensor containing off-diagonal terms appears as

$$\vec{\mu} = \mu_0 \begin{pmatrix} 1+\chi & -i\kappa & 0 \\ i\kappa & 1+\chi & 0 \\ 0 & 0 & 1 \end{pmatrix}, \tag{1}$$

where μ_0 is the permeability of free space and χ is the magnetic susceptibility of the ferromagnet, which is related to the magnetic permeability tensor by $\vec{\mu} = \mu_0(\vec{1} + \vec{\chi})$.

When any resonant photonic mode exists as a doublet, it is because the $\{^{\cos(m\phi)}_{\sin(m\phi)}\}$ degeneracy has been broken by some backscatterer, and the two resulting modes exist as counterpropagating traveling waves [26,40]. The overall effect is that one traveling wave will see an effective permeability of $\mu_+ = \mu_0(1 + \chi + \kappa)$, while the other will see $\mu_- = \mu_0(1 + \chi - \kappa)$, which can be rewritten as $\mu_\pm = \mu_0(1 + \chi_\pm)$, and we can state that $(\chi_+ + \chi_-)/2 = \chi$, where χ is the "unperturbed" magnetic susceptibility that a standing wave would observe.

The effective susceptibility that a mode experiences will determine the interaction strength of that mode with a magnon resonance according to [5]

$$g_i^2 = \chi_{\text{eff}}\omega^2\xi, \tag{2}$$

where ξ is the total magnetic filling factor of the mode, i.e., the proportion of magnetic field within the ferromagnetic material compared to the entire system. This parameter is used in an attempt to quantify the overlap of the magnon and photon modes and is calculated as

$$\xi = \frac{\int\int\int_{V_{\text{YIG}}} \mu_0 \vec{H}^* \vec{H} dV_{\text{YIG}}}{\int\int\int_V \mu_0 \vec{H}^* \vec{H} dV}. \tag{3}$$

It should be noted that typically it is only the magnetic field energy density perpendicular to the external magnetic field that is considered to interact with the spin system [5,21]. However, the interaction of mode 1 is far larger than its perpendicular filling factor of 0.075 would suggest. So, in an attempt to account for the interaction with nonuniform magnon modes, the total magnetic filling factor has been used. These have been calculated from the FEM and the resulting values of χ_{eff} are displayed in Table III.

TABLE III. Calculated magnetic filling factors ξ_j and effective magnetic susceptibilities χ_{eff} for each of the photon modes.

Mode	$\omega_{j\|B\to 7\,\text{T}}/2\pi$ (GHz)	g_j/π (GHz)	ξ_j	χ_{eff}
x	12.779	4.79	0.221	0.159
i	15.506	7.11	0.594	0.0885
ii	15.563	4.19	0.594	0.0305
1	15.732	6.15	0.728	0.0525
2	15.893	3.04	0.493	0.0185
3	15.950	0.78	0.493	0.00121

Given our assumption that mode 1 represents the (1,0) dielectric mode, which will exist as a standing wave given no possible degeneracy, the calculated χ_{eff} value for this mode should represent the unperturbed magnetic susceptibility of the YIG. Taking the average of the χ_{eff} values for the doublet modes i (χ_+) and ii (χ_-) yields a value of $\chi = 0.059\,5$, in reasonable agreement with the value obtained from mode 1.

The FEM predicts that modes x, 2, and 3 will each contain a significant proportion of magnetic field energy within the sapphire support, so one would expect these modes to observe a lower effective magnetic susceptibility, which would appear true for the latter two modes (their average susceptibility yields an unperturbed susceptibility of ~0.01). However, mode x demonstrates a much larger coupling strength than what should be afforded a mode with its filling factor, hence resulting in a χ_{eff} value approximately 3 times larger than the unperturbed value obtained from modes i,ii, and 1. This suggests that our approximation of using the total magnetic filling factor to quantify the overlap of the magnon and photon modes is not entirely accurate. To accurately explain the origins of the differing interaction strengths of each mode, knowledge of higher-order, nonuniform magnon mode shapes are required in order to replace the filling factor approximation with an overlap value. Unlike Zhang *et al.*'s [4] ultrastrong coupling results with a $d = 2.5$ mm YIG sphere, in which higher-order magnon modes mostly couple weakly with the microwave cavity, here we excite internal, nonuniform electromagnetic resonances, so it is more likely than not that these modes will couple more strongly to nonuniform magnon modes if their mode shapes match up well spatially. The derived values of susceptibility in Table III agree within an order of magnitude to previously measured results [41] but have been underestimated due to the use of filling factor as opposed to a mode overlap integral.

Finally, we can use the predicted mode frequencies of the FEM to determine the permittivity of the YIG sample by varying $\epsilon_{\text{YIG}}/\epsilon_0$ until the frequencies match the asymptotic values measured at high magnetic fields. At these magnetic field values, the matrix in Eq. (1) becomes the identity matrix [41]. By measuring the depth of the sapphire concavity and

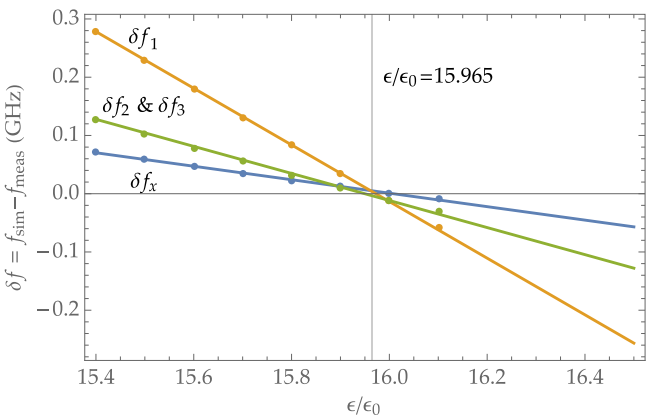

FIG. 10. Frequency difference between simulated and measured results as the relative permittivity of YIG is varied in the FEM software. The radius of curvature of the sapphire support used here was $r' = 3.7$ mm, which for mode 1 is largely irrelevant but for modes x, 2, and 3 gives good agreement.

its width at the surface, the radius of curvature was determined to be $r' = 3.71 \pm 0.2$ mm. With this information, an iterative simulation was conducted mapping mode frequencies versus relative permittivity of YIG. It was found that mode 1 is relatively insensitive to the radius of curvature of the sapphire support. This is due to the absence of electric field density outside the YIG for this particular mode. Given that r' contains a significant amount of uncertainty, this mode is used to match f_{sim} with f_{meas}. A plot of $\delta f = f_{\text{sim}} - f_{\text{meas}}$ versus permittivity is shown in Fig. 10. From this result, we can state that $\epsilon_{\text{YIG}}/\epsilon_0 = 15.96 \pm 0.02$. This value agrees well with previous measurements taken using the so-called "Courtney" technique with YIG samples [42].

V. CONCLUSION

In conclusion, we observe ultrastrong coupling between internal dielectric microwave resonances and magnons inside a $d = 5$ mm YIG sphere. The large diameter of the sphere results in not only an increased number of spins, but also the accessibility of the internal electromagnetic resonances due to their existence below K-band frequencies. The use of internal microwave modes instead of an external cavity resonance results in far larger magnetic filling factors than ever before achieved in such an experiment; hence the coupling values and cooperativity values observed are, to the authors' knowledge, the largest ever reported, with a maximum of $g/\pi = 7.11$ GHz, or ~7000 mode linewidths, and $C = 1.5 \times 10^7$. This implies an extremely high level of coherence in this system. Most importantly, however, the numerous resonant magnon peaks in the dispersive regime and the discrepancies in calculated susceptibilities suggest that higher-order magnon modes participate in this system. This implies that the previously theoretically analyzed models of such systems are incomplete.

ACKNOWLEDGMENT

This work was supported by Australian Research Council Grant No. CE110001013.

[1] A. V. Chumak, V. I. Vasyuchka, A. A. Serga, and B. Hillebrands, Magnon spintronics, Nat. Phys. **11**, 453 (2015).
[2] Y. Tabuchi, S. Ishino, A. Noguchi, T. Ishikawa, R. Yamazaki, K. Usami, and Y. Nakamura, Coherent coupling between a ferromagnetic magnon and a superconducting qubit, Science **349**, 405 (2015).
[3] Y. Tabuchi, S. Ishino, T. Ishikawa, R. Yamazaki, K. Usami, and Y. Nakamura, Hybridizing Ferromagnetic Magnons and Microwave Photons in the Quantum Limit, Phys. Rev. Lett. **113**, 083603 (2014).
[4] X. Zhang, C.-L. Zou, L. Jiang, and H. X. Tang, Strongly Coupled Magnons and Cavity Microwave Photons, Phys. Rev. Lett. **113**, 156401 (2014).
[5] M. Goryachev, W. G. Farr, D. L. Creedon, Y. Fan, M. Kostylev, and M. E. Tobar, High-Cooperativity Cavity QED with Magnons at Microwave Frequencies, Phys. Rev. Appl. **2**, 054002 (2014).
[6] L. Bai, M. Harder, Y. P. Chen, X. Fan, J. Q. Xiao, and C.-M. Hu, Spin Pumping in Electrodynamically Coupled Magnon-Photon Systems, Phys. Rev. Lett. **114**, 227201 (2015).
[7] H. Huebl, C. W. Zollitsch, J. Lotze, F. Hocke, M. Greifenstein, A. Marx, R. Gross, and S. T. B. Goennenwein, High Cooperativity in Coupled Microwave Resonator Ferrimagnetic Insulator Hybrids, Phys. Rev. Lett. **111**, 127003 (2013).
[8] X. Zhang, C.-L. Zou, N. Zhu, F. Marquardt, L. Jiang, and H. X. Tang, Magnon dark modes and gradient memory, Nat. Commun. **6**, 8914 (2015).
[9] A. Imamoğlu, Cavity QED Based on Collective Magnetic Dipole Coupling: Spin Ensembles as Hybrid Two-Level Systems, Phys. Rev. Lett. **102**, 083602 (2009).
[10] X. Zhang, N. Zhu, C.-L. Zou, and H. X. Tang, arXiv:1510.03545.
[11] A. Osada, R. Hisatomi, A. Noguchi, Y. Tabuchi, R. Yamazaki, K. Usami, M. Sadgrove, R. Yalla, M. Nomura, and Y. Nakamura, Cavity optomagnonics with spin-orbit coupled photons, arXiv:1510.01837.
[12] Y. R. Shen and N. Bloembergen, Interaction between light waves and spin waves, Phys. Rev. **143**, 372 (1966).
[13] S. O. Demokritov, B. Hillebrands, and A. N. Slavin, Brillouin light scattering studies of confined spin waves: Linear and nonlinear confinement, Phys. Rep. **348**, 441 (2001).
[14] C. Kittel, Excitation of spin waves in a ferromagnet by a uniform rf field, Phys. Rev. **110**, 1295 (1958).
[15] X. Zhang, C.-L. Zou, L. Jiang, and H. X. Tang, Cavity magnomechanics, Science Advances **2**, e1501286 (2016).
[16] L. Tian, P. Rabl, R. Blatt, and P. Zoller, Interfacing Quantum-Optical and Solid-State Qubits, Phys. Rev. Lett. **92**, 247902 (2004).
[17] J. Verdú, H. Zoubi, Ch. Koller, J. Majer, H. Ritsch, and J. Schmiedmayer, Strong Magnetic Coupling of an Ultracold Gas to a Superconducting Waveguide Cavity, Phys. Rev. Lett. **103**, 043603 (2009).
[18] Z.-L. Xiang, S. Ashhab, J. Q. You, and F. Nori, Hybrid quantum circuits: Superconducting circuits interacting with other quantum systems, Rev. Mod. Phys. **85**, 623 (2013).
[19] V. Cherepanov, I. Kolokolov, and V. Lvov, The saga of YIG: Spectra, thermodynamics, interaction, and relaxation of magnons in a complex magnons, Phys. Rep. **229**, 81 (1993).
[20] A. G. Gurevich, *Ferrites at Microwave Frequencies* (Consultants Bureau, New York, 1963).
[21] Ö. O. Soykal and M. E. Flatté, Strong Field Interactions Between a Nanomagnet and a Photonic cavity, Phys. Rev. Lett. **104**, 077202 (2010).
[22] Ö. O. Soykal and M. E. Flatté, Size dependence of strong coupling between nanomagnets and photonic cavities, Phys. Rev. B **82**, 104413 (2010).
[23] N. Kostylev, M. Goryachev, and M. E. Tobar, Superstrong coupling of a microwave cavity to YIG magnons, Appl. Phys. Lett. **108**, 062402 (2016).
[24] B. Zare Rameshti, Y. Cao, and G. E. W. Bauer, Magnetic spheres in microwave cavities, Phys. Rev. B **91**, 214430 (2015).
[25] W. G. Farr, D. L. Creedon, M. Goryachev, K. Benmessai, and M. E. Tobar, Ultrasensitive microwave spectroscopy of paramagnetic impurities in sapphire crystals at millikelvin temperatures, Phys. Rev. B **88**, 224426 (2013).

[26] M. Goryachev, W. G. Farr, D. L. Creedon, and M. E. Tobar, Spin-photon interaction in a cavity with time-reversal symmetry breaking, Phys. Rev. B **89**, 224407 (2014).

[27] J. Bourhill, K. Benmessai, M. Goryachev, D. L. Creedon, W. Farr, and M. E. Tobar, Spin bath maser in a cryogenically cooled sapphire whispering gallery mode resonator, Phys. Rev. B **88**, 235104 (2013).

[28] J. Bourhill, M. Goryachev, W. G. Farr, and M. E. Tobar, Collective behavior of Cr^{3+} ions in ruby revealed by whispering gallery modes, Phys. Rev. A **92**, 023805 (2015).

[29] W. G. Farr, M. Goryachev, D. L. Creedon, and M. E. Tobar, Strong coupling between whispering gallery modes and chromium ions in ruby, Phys. Rev. B **90**, 054409 (2014).

[30] P. Del'Haye, A. Schliesser, O. Arcizet, T. Wilken, R. Holzwarth, and T. J. Kippenberg, Optical frequency comb generation from a monolithic microresonator, Nature (London) **450**, 1214 (2007).

[31] T. J. Kippenberg, J. Kalkman, A. Polman, and K. J. Vahala, Demonstration of an erbium-doped microdisk laser on a silicon chip, Phys. Rev. A **74**, 051802 (2006).

[32] M. Aspelmeyer, T. J. Kippenberg, and F. Marquardt, Cavity optomechanics, Rev. Mod. Phys. **86**, 1391 (2014).

[33] J. Bourhill, E. Ivanov, and M. E. Tobar, Precision measurement of a low-loss cylindrical dumbbell-shaped sapphire mechanical oscillator using radiation pressure, Phys. Rev. A **92**, 023817 (2015).

[34] E. N. Ivanov and M. E. Tobar, Microwave phase detection at the level of 10(-11) radRev. Sci. Instrum. **80**, 044701 (2009).

[35] E. N. Ivanov and M. E. Tobar, Low phase-noise sapphire crystal microwave oscillators: Current status, IEEE Trans. Ultrason. Ferroelectr. Freq. Control **56**, 263 (2009).

[36] A. A. Serga, C. W. Sandweg, V. I. Vasyuchka, M. B. Jungfleisch, B. Hillebrands, A. Kreisel, P. Kopietz, and M. P. Kostylev, Brillouin light scattering spectroscopy of parametrically excited dipole-exchange magnons, Phys. Rev. B **86**, 134403 (2012).

[37] W. G. Farr, M. Goryachev, J.-M. le Floch, P. Bushev, and M. E. Tobar, Evidence of dilute ferromagnetism in rare-earth doped yttrium aluminium garnet, Appl. Phys. Lett. **107**, 122401 (2015).

[38] M. Goryachev, W. G. Farr, D. L. Creedon, and M. E. Tobar, Controlling a whispering-gallery-doublet-mode avoided frequency crossing: Strong coupling between photon bosonic and spin degrees of freedom, Phys. Rev. A **89**, 013810 (2014).

[39] J.-M. le Floch, J. D. Anstie, M. E. Tobar, J. G. Hartnett, P.-Y. Bourgeois, and D. Cros, Whispering modes in anisotropic and isotropic dielectric spherical resonators, Phys. Lett. A **359**, 1 (2006).

[40] K. Benmessai, M. E. Tobar, N. Bazin, P.-Y. Bourgeois, Y. Kersalé, and V. Giordano, Creating traveling waves from standing waves from the gyrotropic paramagnetic properties of Fe^{3+} ions in a high-q whispering gallery mode sapphire resonator, Phys. Rev. B **79**, 174432 (2009).

[41] J. Krupka, Measurements of all complex permeability tensor components and the effective line widths of microwave ferrites using dielectric ring resonators, IEEE Trans. Microwave Theory Tech. **39**, 1148 (1991).

[42] J. Krupka, S. A Gabelich, K. Derzakowski, and B. M. Pierce, Comparison of split post dielectric resonator and ferrite disk resonator techniques for microwave permittivity measurements of polycrystalline yttrium iron garnet, Meas. Sci. Technol. **10**, 1004 (1999).